A general method for calculating the traffic load-induced residual settlement of a platform, based on a structural analysis approach

M. Abdelkrim, Patrick de Buhan, Guy Bonnet

A GENERAL METHOD FOR CALCULATING THE TRAFFIC LOAD-INDUCED RESIDUAL SETTLEMENT OF A PLATFORM, BASED ON A STRUCTURAL ANALYSIS APPROACH

M. ABDELKRIM[i], P. DE BUHAN[ii] and G. BONNET[iii]

ABSTRACT

A general computational procedure is developed in this paper for calculating the long term response, and more specifically the evolution with time of the accumulated residual settlement of a traffic platform under the action of repeated vehicle loading. It is based on a structural analysis approach, which incorporates as an essential feature, the use of a cyclic constitutive law for the constituent materials, formulated on the basis of cyclic triaxial tests. A numerical tool has been set up with the help of a finite element code, in order to simulate experimental tests performed on reduced scale models of a railway track platform. A first comparison is being made between the numerical simulations and the experimental results, as regards the long term evolution of the residual settlement.

Key words: permanent deformations, residual settlement, traffic loading, unbound granular materials (**IGC**: E2/E11/E13)

INTRODUCTION

Appropriate design and maintenance procedures for transportation infrastructures, such as road pavements or railway track platforms, should rely on computational methods allowing to predict the long term performance of this kind of structures, and notably the residual surface settlement of the infrastructure (pavement rutting, track geometry defects) due to the application of repeated traffic loading. The somewhat complex phenomena involved in this kind of geotechnical structures could be analyzed by resorting to experiments. Specific experimental devices have for instance been set up for testing representative sections of road pavements subject to repeated wheel loading. More recently, in the field of railway technology, an extensive experimental program has been carried out on reduced scale models simulating a representative section of ballast railway track platform subject to cyclic loading (Guérin, 1996; Bodin, 2001; Indraratna and Salim, 2003). Such experimental approaches are undoubtedly useful for obtaining a preliminary global understanding of the problem, at least from a qualitative point of view, even making it possible to derive empirical relationships giving for instance the amount of residual settlement as a function of the number of applied load cycles (up to several millions). However, they remain inadequate for providing really predictive design methods over a wide range of parameters.

The general method and related numerical tool developed in this paper are based on a "structural analysis" point of view. According to this point of view, the response of a traffic platform, and more specifically its residual surface settlement, may be derived as the solution of a boundary value problem, provided that the local constitutive behaviour of the materials has been previously characterised in terms of stress-strain relationships. More precisely, considering the particular kind of loading involved in the analysis, it clearly appears that such constitutive relationships will refer to the long term cyclic behaviour of the different constituent materials, which exhibit irreversible permanent deformations under cyclic solicitations.

As recently pointed out by Niemunis et al. (2004) or Wichtmann et al. (2005), two different approaches may be considered for formulating such a cyclic constitutive behaviour. The first one, which may be called "implicit", would consist in implementing a conventional step-by-step elastoplastic procedure, requiring the discretisation of each individual load cycle into sufficiently small increments. It is clear that such a numerical strategy, which may prove valid for a relatively small number of cycles (say a few tens), will quite rapidly lead to considerable computational time and complete loss of numerical accuracy as the number of cycles increases. The alternative "explicit" or "N-type" approach advocated in the present paper, is aimed at establishing a direct relationship between the amount of permanent deformations

[i] Civil Engineering Laboratory, Ecole Nationale des Ingénieurs de Tunis, Tunis, Tunisia.
[ii] Laboratoire des Matériaux et Structures du Génie Civil (LCPC, ENPC, CNRS UMR 113), France (debuhan@lmsgc.enpc.fr).
[iii] Laboratoire de Mécanique, Institut Navier, Université de Marne-la-Vallée, France.

exhibited by the materials subject to cyclic loading, and the number N of applied cycles, as well as the characteristics of the latter, such as its amplitude, position with repect to the failure line, etc.

Such an explicit cyclic constitutive law is to be identified experimentally, by means of repeated load triaxial tests performed on homogeneous specimens of materials. Monosmith et al. (1975) for instance, or Li and Selig (1996), have proposed such formulations relating the accumulated permanent strain of cohesive subsoils subject to repeated loading, to the number of load cycles, as well as some relevant characteristics of the stress cycle. Simplified methods, making use of such formulations, have been set up for predicting the residual response of road pavements (Chai and Miura, 2002) or railway track platforms (Li and Selig, 1998). Similar cyclic constitutive laws have also been proposed for granular cohesionless materials, such as railroad ballast (Raymond and Williams, 1978; Alva-Hurtado, 1980), or unbound granular materials in the context of road pavement construction (Hornych et al., 1993; Lekarp and Dawson, 1998; Gidel et al., 2001). Quite recently, an intensive experimental research program has been undertaken with the objective of formulating an explicit cyclic law for a sand subject to more or less complex cyclic stress paths (Wichtmann et al., 2004; Niemunis et al., 2005).

The principle of a structural analysis-based methodology has been outlined in a previous paper (Abdelkrim et al., 2003), resulting from the incorporation of such a cyclic constitutive law into a calculation procedure. The whole methodology was illustrated on the simplified configuration of a moving strip-load acting upon a half-space, where an analytical treatment was possible. The present paper proposes further improvements of the initial procedure on the two following points. First, the tensorial formulation of the cyclic constitutive law, which makes it possible to integrate the numerical procedure into a finite element computer code. Second, the possibility to account for the elastoplastic (and not only the elastic) properties of the materials in the analysis.

The paper is decomposed into three main successive parts:

- ◇ The principles of the general computational procedure aimed at predicting the long term behaviour of a traffic platform under repeated vehicle loads, is first recalled, starting from a preliminary analysis of the platform settlement as a double time-scale phenomenon (sections 2 and 3).
- ◇ A detailed description of a cyclic constitutive law for unbound granular materials, from its initial formulation identified from radial stress cycles, to its extension to more complex three-dimensional loading paths is then presented (section 4).
- ◇ Finally, the application to the simulation of experimental tests performed on a reduced scale model of a ballast track platform is carried out, first by resorting to a simplified analytical model, then by making use of a numerical tool specifically developed in the framework of an existing finite element code (sections 5 and 6).

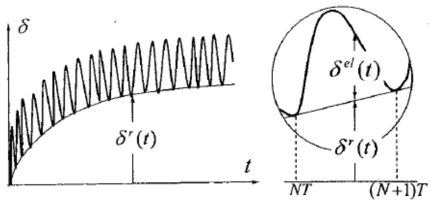

Fig. 1. Evolution of the global settlement of a platform subject to repeated traffic loading, as a double time scale phenomenon

PRELIMINARY ANALYSIS

Settlement of a Platform Infrastructure

Figure 1 represents the typical response of a road pavement or railway structure under traffic loading, namely the evolution of the vertical settlement δ at a particular point, as a function of time t, comprised between NT and $(N+1)T$, where N is the number of applied wheel loads due to the passage of vehicles, and T is the period between two such successive loads. It should be noted that there is no need to further specify the latter quantity, since visco-elastic effects will not be considered in the subsequent analysis, hence the only relevant loading parameter is the number N of load cycles, and not the actual time t during which they are applied. More precisely, the following additive decomposition may be postulated;

$$\delta(t)=\delta^{el}(t)+\delta^{r}(t) \tag{1}$$

where the first term denotes the rapidly fluctuating elastic deflection which vanishes as the load is removed (that is as the vehicle is moving far away from the point where the settlement is measured), while the second term represents the residual settlement, which is slowly increasing with time. It is clearly apparent from such a figure, that the increment of residual settlement over one period of time (say $t\in\lfloor NT,\,(N+1)T\rfloor$), is considerably smaller than the maximum amplitude of the elastic deflection over the same period:

$$\delta^{r}((N+1)T)-\delta^{r}(NT) \ll \text{Max}\,\{\delta^{el}(t),\ t\in[NT,\,(N+1)T]\} \tag{2}$$

so that the settlement could be viewed as a *quasi-periodic* function of time. But it should also be emphasised that, despite its slow variation, the accumulated residual settlement over a very large number of load cycles (up to several millions cycles), may be of the same order, or even greater, than the elastic deflection.

Local Response of Materials

The same kind of analysis could be performed *locally*, that is at any point $\underline{x}$ of the structure. Indeed, the stress state at such a point may be written as the superposition of an *elastic* (recoverable) component due to the applied

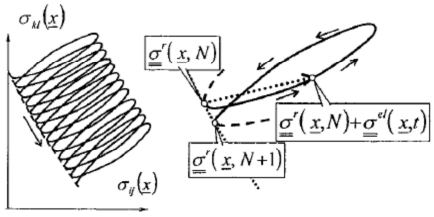

Fig. 2. Stress path at any point of the structure

load and a *residual* stress:

$$\underline{\sigma}(\underline{x}, t)=\underline{\sigma}^{el}(\underline{x}, t)+\underline{\sigma}^r(\underline{x}, t) \tag{3}$$

Let us then consider the path followed by such a stress state in the space of stresses, as sketched in Fig. 2. It may be drawn as a continuous chain of loops corresponding to the elastic load cycle slowly drifting in the stress space as the number N of applied load cycles increases. The distance between two such successive loop-cycles appears to be quite small when compared with the loop size itself. In other terms, the increment of the residual stress per load-cycle is negligible in comparison with the maximum amplitude of the elastic cycle:

$$\|\underline{\sigma}^r(\underline{x}, (N+1)T)-\underline{\sigma}^r(\underline{x}, NT)\| \ll \text{Max}\{\|\underline{\sigma}^{el}(t)\|,\ t\in[NT,\ (N+1)T]\} \tag{4}$$

Again, it should be kept in mind that the total amount of residual settlement accumulated at the end of a very large number of load-cycles may result in the same order as the elastic stress amplitude.

Mechanical Background

The above described *two time-scale* evolution of the settlement of a traffic-platform under repeated loading, is somewhat reminiscent of the liquefaction phenomenon of soil masses subject to seismic or wave loading (*see* for instance Dormieux et al., 1993, or Pecker et al., 2001). Indeed, as already pointed out, this evolution may be described by a quasi-periodic function of time, in much the same way as, in a quite different context, the curves representing the evolution of excess pore pressure progressively building up in a saturated granular soil sample subject to deviatoric cyclic loading, ultimately triggering liquefaction when the effective stress drops to zero. It has been clearly shown that the underlying physical explanation of such a progressive accumulation of excess pore pressure and subsequent liquefaction, is to be found in the soil's volume decrease (contraction) generated by cyclic loading (Dormieux et al., 1993).

The fundamental assumption upon which the analysis and related design method developed in this paper are based, is that the long term behaviour of a traffic platform, observed at both the global (progressive accumulation of residual settlement) and local levels (drift of residual stresses), is to be attributed to the cyclic behaviour of the different constituent granular materials (ballast, gravel, cohesionless soils, etc.). More precisely, it turns out that those materials undergo irreversible deformations, called *permanent* deformations, when subjected to repeated loadings, as shown for instance by Alva-Hurtado (1980) and Hornych et al. (1993), who performed repeated triaxial tests on ballast material and pavement unbound granular materials, respectively.

SETTING UP A GENERAL CALCULATION PROCEDURE (Abdelkrim et al., 2003)

The fundamental starting point for setting up a general calculation procedure aimed at predicting the residual settlement of a platform under repeated traffic loading, lies in the formulation of a constitutive law for the different materials subject to cyclic loading. Such a cyclic constitutive law may be expressed in the form of a local relationship between the rate of accumulation of permanent strain at the N^{th} load cycle and the characteristics of the cyclic loading path, namely:

$$\frac{d\underline{\underline{\varepsilon}}^*}{dN}(\underline{x}, N)=F\left[N;\ \left\{\oint \underline{\sigma}\right\}(\underline{x}, N)\right] \tag{5}$$

where:

- ◇ $\underline{\underline{\varepsilon}}(\underline{x}, N)$ is the *permanent* strain experienced by the material located at point $\underline{x}$ at the end of N applied cycles;
- ◇ and $\{\int \underline{\sigma}\}(\underline{x}, N)$ denotes the stress cycle to which the material located at the same point $\underline{x}$ is submitted at the same time $t=NT$.

The method developed hereafter is based on two main assumptions:

a) The short term reversible behaviour of the different materials is described by a linear elastic constitutive law.

b) The elastic stiffness parameters (that is the Young modulus and Poisson ratio in the case of isotropic materials) remain unaffected by the cyclic loading. This means that neither damage nor stiffening is taken into account in the analysis.

While the second assumption appears to be reasonably well verified, at least after small number of load cycles has been applied, the first assumption however, seems more questionable, since experimental evidence of a strong non linearity has been given for some granular materials (Boyce, 1980). More importantly, as it will be seen later on, plastic, and not only elastic properties, should be incorporated in the materials short term response.

As an important consequence of theses hypotheses, it appears from the application of the superposition principle, that the current stress cycle actually applied to the material is obtained in the stress space from translating a so called *reference* stress cycle by the residual stress (Fig. 3), which may be written as:

$$\left\{\oint \underline{\sigma}\right\}(\underline{x}, N)=\underline{\sigma}^r(\underline{x}, N)+\left\{\oint \underline{\sigma}\right\}^{\text{ref}}(\underline{x}) \tag{6}$$

It is to be noted that the *reference* stress cycle is a function of point $\underline{x}$ only. It is simply obtained as the continuous sequence of stress states generated at that same point

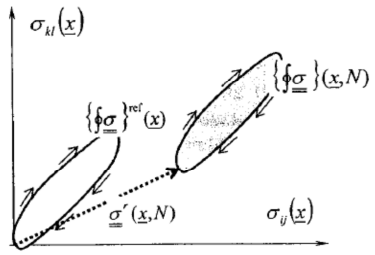

Fig. 3. Reference and current stress cycles at point $\underline{x}$

as the load is moving on the platform surface, which may be derived from the solution of a simple elastic boundary value problem. The latter problem can be solved under either quasistatic or dynamic conditions, depending on the velocity of the moving load (case of high speed trains in railway traffic).

It appears from this preliminary analysis that the proposed method should combine three complementary elements:

(i) The formulation of a cyclic constitutive law in the form of Eq. (5), which has to be derived from laboratory tests conducted for each type of material and for various cyclic loading conditions.

(ii) A computational tool for determining the reference stress cycle at any point of the structure as a function of the traffic loading characteristics.

(iii) A numerical procedure for calculating the residual state of the structure, and more particularly the residual settlement, from the knowledge of the accumulated distribution of permanent strains.

Procedure (iii) amounts to solving an elastic boundary value problem relating to the same structure, in the absence of the traffic load, but with the permanent strain distribution acting as a *prescribed non-elastic* strain field, in exactly the same way as for thermal or plastic strains. The existence, and subsequent evolution, of the residual stress field is thus clearly connected with the geometrical non-compatibility of this strain field.

Due to the rate-type or incremental formulation (5) of the cyclic constitutive law, the implementation of such a method requires the discretisation of the total number of applied load cycles into a finite number of increments. The principle of the corresponding numerical algorithm, which is sketched in Fig. 4, may therefore be described as follows:

◇ A first loading-unloading cycle is applied to the structure, taking into account the elastoplastic properties of the materials, leading to an updated initial state ($N=1$) from the initial one ($N=0$), with the objective to obtain a first quasi elastic cycle upon reloading from the updated initial state.

◇ The step-by-step algorithm is getting started from $N=1$, where the permanent strain field and associated residual settlement are conventionally taken equal to zero, while the residual stress field is equal to the updated initial stress field, which must be in equilibrium with the gravity loads.

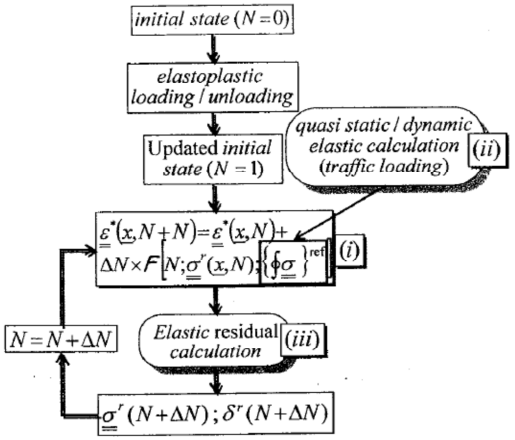

Fig. 4. Step-by-step calculation procedure for determining the evolution of the residual platform settlement

◇ Assuming now that the permanent strain field, along with the residual state, are being known up to N cycles. The local value of the permanent strain field for $N+\Delta N$ cycles is simply computed as the sum of its value at the previous step and of the increment, given by Eq. (5), so that:

$$\underline{\underline{\varepsilon}}^*(\underline{x}, N+\Delta N)=\underline{\underline{\varepsilon}}^*(\underline{x}, N)+\Delta N \times F\left[N;\ \underline{\underline{\sigma}}^r(\underline{x}, N)+\left\{\oint \underline{\underline{\sigma}}\right\}^{ref}(\underline{x})\right] \quad (7)$$

◇ The values of the residual stresses, strains and settlements are then updated for $N+\Delta N$ cycles from an elastic residual calculation.

Adopting a cyclic constitutive law, such as that which will now be presented in detail, the implementation of such a calculation procedure has been illustrated in Abdelkrim et al. (2003) on the example of a moving strip-load acting on a homogeneous half-space, where all calculations may be carried out analytically.

FORMULATION OF AN EXPLICIT CONSTITUTIVE CYCLIC LAW

The implementation of the above-described general method requires the use of a cyclic constitutive law, connecting the amount of permanent deformations exhibited by the materials under repeated loading, to the number of loading cycles, as well as to some cycle's characteristics, such as its position and amplitude in the stress-space. Such a model will first be presented in its initial version, then generalized.

Description of the Initial Model

The cyclic constitutive law we shall adopt in the present analysis, is straightforwardly derived from that formulated by Hornych et al. (1993) and more recently Gidel et al. (2001), on the basis of triaxial tests performed on

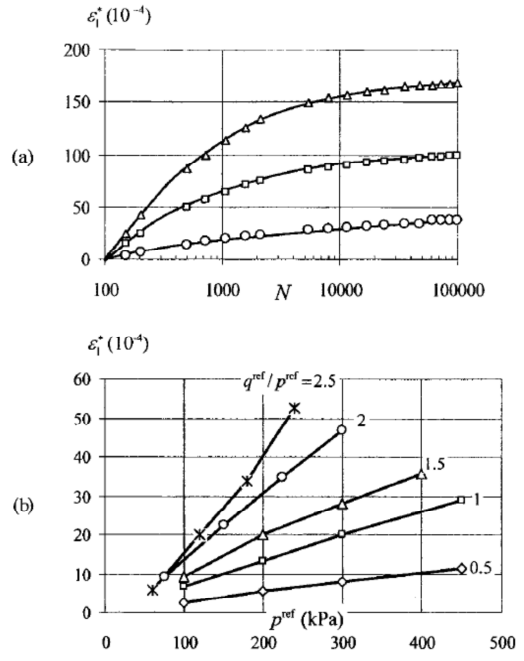

Fig. 5. (a) Accumulated axial permanent strain as a function of the number of applied stress cycles (experimental results from Hornych et al. (1993)) and (b) Influence of the stress cycle characteristics on the amount of permanent strain accumulated between 100 and 20000 cycles (experimental results from Gidel et al. (2001))

samples of unbound granular materials (UGM), used for instance in the construction of pavements, which were submitted to *radial* stress cycles. Figure 5(a) for example displays a series of experimental results obtained by Hornych et al. (1993) giving the evolution of the permanent axial or vertical strain ε_1^* accumulated between 100 cycles and N cycles for different stress levels. The solid lines in the same figure correspond to the curves drawn by the same authors according to a power law variation of the form:

$$\varepsilon_1^*(N) = A(1-(N/100)^{-B}) \tag{8}$$

which turned out to best fit the experimental points.

A few comments deserve to be made with regards to such a proposed cyclic constitutive law. One of the main issues to be raised when proposing such a formulation, concerns the way the axial permanent deformation is increasing as a function of the number N of cycles. For particular triaxial loading paths conducted on ballast materials, where the confining pressure is kept constant, Alva-Hurtado (1980) for instance, proposes a variation of the form $a+b\mathrm{Ln}N$, while Li and Selig (1996) suggest a power-law variation of the form aN^b. Unlike the above formulation (8), which is also adopted by Lekarp and Dawson (1998), the latter formulas implicitly assume that there is no stabilization of the accumulated permanent deformations. Actually, this remains an open question which could only be settled by performing repeated load

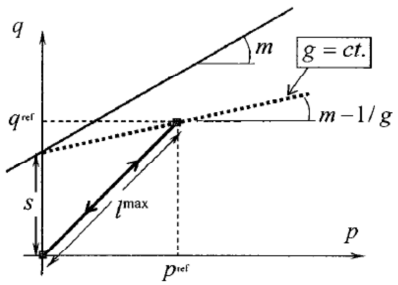

Fig. 6. Representation of the cyclic constitutive law proposed by Gidel et al. (2001) in the (p, q)-plane for radial stress paths

triaxial tests up to several millions cycles, whereas in most experiments the number of applied stress cycles does not exceed a few hundreds of thousands. Referring to the proposed law (8), the coefficient A represents the asymptotic value of the axial permanent deformation obtained when N tends to infinity. In the case when the exponent B is small with respect to unity (say less than 0.1), such an asymptotic value may be never reached in practice.

Furthermore, performing an extensive experimental programme on the same unbound granular materials, Gidel et al. (2001) have investigated the dependence of the accumulated permanent strain amplitude for a given number of applied cycles on the stress path characteristics, namely their maximum loading point (p^{ref}, q^{ref}) in the (p, q)-plane (*see* Fig. 6), with:

$$p = -1/3\mathrm{tr}\underline{\underline{\sigma}} \text{ and } q = (3/2\ \underline{\underline{s}}:\underline{\underline{s}})^{1/2} \text{ where } \underline{\underline{s}} = \underline{\underline{\sigma}} + p\underline{\underline{1}} \tag{9}$$

Figure 5(b) illustrates for instance the different values of the axial permanent strain experienced by a same material between $N=200$ and 20000 cycles, as a function of the maximum mean stress p^{ref}, as well as of the inclination q^{ref}/p^{ref} of the radial stress path. As a result of this parametric experimental study, Gidel et al. (2001) have finally proposed the following expression;

$$\varepsilon_1^*(N) = \varepsilon_0^*[1-(N/100)^{-B}]f(p^{ref}, q^{ref})g(p^{ref}, q^{ref}) \tag{10}$$

where

$$f(p^{ref}, q^{ref}) = (l^{max}/100)^n \text{ with } l^{max} = \sqrt{(p^{ref})^2+(q^{ref})^2}$$

$$g(p^{ref}, q^{ref}) = \frac{p^{ref}}{s+mp^{ref}-q^{ref}} \tag{11}$$

ε_0^*, B, n, s and m being material parameters, while all the stress quantities are expressed in kPa.

Function f represents the influence of the stress cycle amplitude on the amount of permanent strain, while function g quantifies the proximity of the maximum loading point with respect to a "*reference line*" of equation $q=s+mp$. More precisely, the contour lines of g are straight lines intersecting the q-axis at the same point as the "reference line", with a slope equal to $m-1/g$, as shown in Fig. 6, so that the value of function g tends to infinity as the peak stress point approaches this reference line.

Since the interest of Gidel et al. (2001) was primarily

focused on the measurement of axial permanent deformations $\varepsilon_1^*(N)$, they did not propose a specific cyclic constitutive law expressing the evolution of *lateral* permanent deformations. However, the analysis of available experimental data tends to suggest that the evolution of these lateral components is similar to that of the axial one. More precisely, it is convenient to introduce the following non-dimensional coefficient;

$$\nu^* = -\frac{\varepsilon_2^*(N)}{\varepsilon_1^*(N)} \tag{12}$$

which could be interpreted as the equivalent of a Poisson's ratio, classically introduced for isotropic elastic materials. Experimental results show that such a coefficient increases with the slope of the stress path, so that, as a first approach, a linear relationship can be proposed in the form;

$$\nu^*\left(\frac{q^{\text{ref}}}{p^{\text{ref}}}\right) = -1 + \kappa\frac{q^{\text{ref}}}{p^{\text{ref}}},\ \kappa > 0 \tag{13}$$

thus taking into account the fact that the lateral and axial permanent strains are equal (*i.e.* $\nu^* = -1$) for an purely isotropic cyclic loading ($q^{\text{ref}}/p^{\text{ref}} = 0$). For the Poulmarch gravel for instance, the cyclic behaviour of which is described in Gidel et al. (2001), the value of parameter κ was found close to 2/3.

Coefficient ν^* may be connected with the notions of dilatancy and contractancy usually introduced in soil mechanics for assessing the volume changes of soils subject to cyclic loading. Indeed, the *permanent volumetric* strain is defined as:

$$\varepsilon_v^*(N) = \text{tr}(\underline{\varepsilon}^*) = \varepsilon_1^* + 2\varepsilon_2^* = (1 - 2\nu^*)\varepsilon_1^* \tag{14}$$

so that, on account of the fact that $\varepsilon_1^* < 0$, it appears that the material is *dilatant* ($\varepsilon_v^* > 0$) for $\nu^* > 1/2$ or $q^{\text{ref}}/p^{\text{ref}} > 3/(2\kappa)$, while it is *contractant* ($\varepsilon_v^* < 0$) in the other case.

Generalizations of the Initial Law

Extension to the Case of Non-radial Cyclic Paths

Although the cyclic constitutive law (8) has been identified on the particular situation of *radial* stress paths, it is necessary to propose its generalisation to non-radial stress-paths. Indeed, due to the accumulation of permanent deformations in materials and the corresponding development of residual stresses, the stress cycle doesn't start from the origin anymore. Furthermore, its shape may be significantly different, as shown in Fig. 6. In the absence of any further experimental evidence, it seems reasonable to propose the following extension of the cyclic constitutive law. We can first define the maximum loading point on the current stress cycle, as that corresponding to the maximum value of function g, as sketched in Fig. 6, and the amplitude of the stress cycle could be defined as:

$$l^{\max} = \sqrt{(p^m - p^r)^2 + (q^m - q^r)^2} \tag{15}$$

where (p^m, q^m) are the co-ordinates of the maximum loading point. The initial cyclic law can thus be changed into:

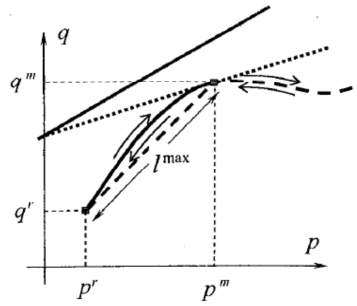

Fig. 7. Extension of the constitutive cyclic law to a non-radial stress cycle

$$\varepsilon_1^*(N) = \varepsilon_0^*(1 - N^{-B}) f(p^m - p^r,\ q^m - q^r) g(p^m,\ q^m) \tag{16}$$

and the increment of axial permanent deformation due to the application of ΔN stress cycles between N and $N + \Delta N$ is then given by

$$\begin{aligned}\Delta\varepsilon_1^*(N) &= \varepsilon_1^*(N + \Delta N) - \varepsilon_1^*(N) \\ &\cong \varepsilon_0^*(N^{-B} - (N + \Delta N)^{-B}) f.g.\end{aligned} \tag{17}$$

in which functions f and g are calculated for N, that is neglecting the drift of the stress cycle due to the variation of the residual stress between N and $N + \Delta N$.

This kind of extension of the initial cyclic law is for instance readily applicable to a structure subjected to a load having a fixed orientation, the amplitude of which being cyclically varied between two extreme values. Indeed, in such a situation the maximum loading point corresponds to the application of the maximum load intensity. This is the case of the experiments conducted on reduced scale models of railway track platforms, such as the BETTER test, which will be simulated later on (section 5).

Extension to Non-triaxial Stress Paths

The constitutive cyclic law, given by Eqs. (10) and (12), being formulated for axisymmetrical triaxial solicitations only ($\sigma_2 = \sigma_3 \geq \sigma_1$)[1], is also necessary for proposing its extension to the case of fully three-dimensional stress cycles, where the three principal stresses may be different. Considering a radial stress cycle of the form:

$$\underline{\sigma} = \eta\underline{\sigma}^{\text{ref}} \tag{18}$$

where η is cyclically varied between 0 and 1, $\underline{\sigma}^{\text{ref}}$ may be written as:

$$\underline{\sigma}^{\text{ref}} = \sigma_1^{\text{ref}}\underline{e}_1 \otimes \underline{e}_1 + \sigma_2^{\text{ref}}\underline{e}_2 \otimes \underline{e}_2 + \sigma_3^{\text{ref}}\underline{e}_3 \otimes \underline{e}_3 \tag{19}$$

where σ_i^{ref}, $i = 1, 2, 3$ are the principal stresses:

$$\sigma_1^{\text{ref}} \leq \sigma_2^{\text{ref}} \leq \sigma_3^{\text{ref}} \tag{20}$$

and σ_1^{ref} the *maximum compressive* stress. Splitting $\underline{\sigma}^{\text{ref}}$ into its deviatoric and spherical parts:

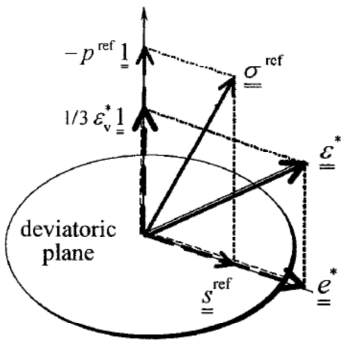

Fig. 8. Decomposition of reference stress and permanent strain tensors into deviatoric and isotropic parts

$$\underline{\sigma}^{ref}=\underline{s}^{ref}-p^{ref}\underline{1} \text{ with } p^{ref}=-\frac{1}{3}\,\mathrm{tr}(\underline{\sigma}^{ref}) \tag{21}$$

and introducing the same decomposition for the permanent strain tensor:

$$\underline{\varepsilon}^*=\underline{e}^*+\frac{1}{3}\,\varepsilon_v^*\underline{1} \text{ with } \varepsilon_v^*=\mathrm{tr}(\underline{\varepsilon}^*) \tag{22}$$

the proposed three-dimensional extension relies upon the assumption that $\underline{\varepsilon}^*$ and $\underline{\sigma}^{ref}$ are located in the same plane passing through the axis of isotropic tensors as shown in Fig. 8, which provides a representation of such tensors as vectors in a six dimensional space, so that the following decomposition can be introduced:

$$\underline{\varepsilon}^*=\alpha\underline{1}+\beta\,\frac{\underline{s}^{ref}}{q^{ref}} \tag{23}$$

$\underline{\varepsilon}^*$ and $\underline{\sigma}^{ref}$ have therefore the same principal directions (Fig. 9):

$$\underline{\varepsilon}^*=\varepsilon_1^*\underline{e}_1\otimes\underline{e}_1+\varepsilon_2^*\underline{e}_2\otimes\underline{e}_2+\varepsilon_3^*\underline{e}_3\otimes\underline{e}_3 \tag{24}$$

Coefficients α and β are then determined by considering the case when both stress and permanent strain tensors are axisymmetric:

$$\varepsilon_2^*=\varepsilon_3^*\geq\varepsilon_1^*,\ \sigma_2^{ref}=\sigma_3^{ref}\geq\sigma_1^{ref} \tag{25}$$

Indeed, in such a situation we get:

$$\underline{s}^{ref}=\frac{\sigma_1^{ref}-\sigma_2^{ref}}{3}\,(2\underline{e}_1\otimes\underline{e}_1-\underline{e}_2\otimes\underline{e}_2-\underline{e}_3\otimes\underline{e}_3) \tag{26}$$

$$q^{ref}=\sigma_2^{ref}-\sigma_1^{ref} \tag{27}$$

hence from (22):

$$\underline{\varepsilon}^*=\alpha\underline{1}+\frac{\beta}{3}\,(-2\underline{e}_1\otimes\underline{e}_1+\underline{e}_2\otimes\underline{e}_2+\underline{e}_3\otimes\underline{e}_3) \tag{28}$$

Identifying the latter equation with (24) yields:

$$\varepsilon_1^*(N;\,p^{ref},\,q^{ref})=\alpha-\frac{2}{3}\beta,\ \varepsilon_2^*=-\nu^*\varepsilon_1^*=\alpha+\frac{\beta}{3} \tag{29}$$

and finally:

$$\alpha=\frac{(1-2\nu^*)}{3}\,\varepsilon_1^*,\ \beta=-(1+\nu^*)\varepsilon_1^* \tag{30}$$

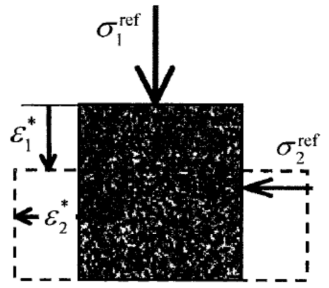

Fig. 9. Maximum stresses and associated permanent strains

Substituting the values of α and β given by Eq. (30) into Eq. (23), provides the following tensorial expression for the permanent deformation;

$$\underline{\varepsilon}^*=\varepsilon_1^*(N;\,p^{ref};\,q^{ref})\left[\frac{1-2\nu^*}{3}\,\underline{1}-(1+\nu^*)\,\frac{\underline{s}^{ref}}{q^{ref}}\right] \tag{31}$$

APPLICATION TO THE SIMULATION OF AN EXPERIMENTAL TEST ON A BALLAST RAILWAY PLATFORM

Description of the Test and Plane Strain Model

Figure 10(a) provides a simplified description of the device used to perform a series of tests carried out by Bodin (2001) (*see* also Bodin et al., 2004). The objective of this experiment was to simulate the response of a ballast railway track subject to the action of traffic loading, by applying to a reduced-scale model of such a railway platform (the dimensions of the model were equal to one third those of the in-situ platform), a cyclically varying force exerted through a pair of concrete sleepers lying on top of the ballast layer. The entire experimental set up was placed into a parallelepipedic box. Referring to an orthonormal frame $Ox_1x_2x_3$, Fig. 10(a) represents a *cross section* of the experimental set up in the Ox_1x_3-plane. The grain size of the ballast material used in the model was scaled down to one third that of the ballast employed in-situ. The effect of the underlying soil is reproduced by incorporating an elastomeric layer placed at the base of the container. Its properties were chosen such as to reproduce the stiffness of the underlying soil. The force applied to the sleepers could be inclined with respect to the vertical, in order to reproduce lateral loading associated with the passage of trains around bends in railway tracks, while sensors were placed on each sleeper in order to measure vertical as well as lateral displacements. Only the case of vertical loading will be considered in the sequel. The evolution of both the elastic deflection and the accumulated residual settlement of the sleepers is then measured as a function of the number of applied load cycles (up to one million).

In order to simulate such a three dimensional structure by means of the finite element code CESAR-LCPC, the problem is first simplified as a *plane strain problem*, taking into account the fact that the sleeper is three times

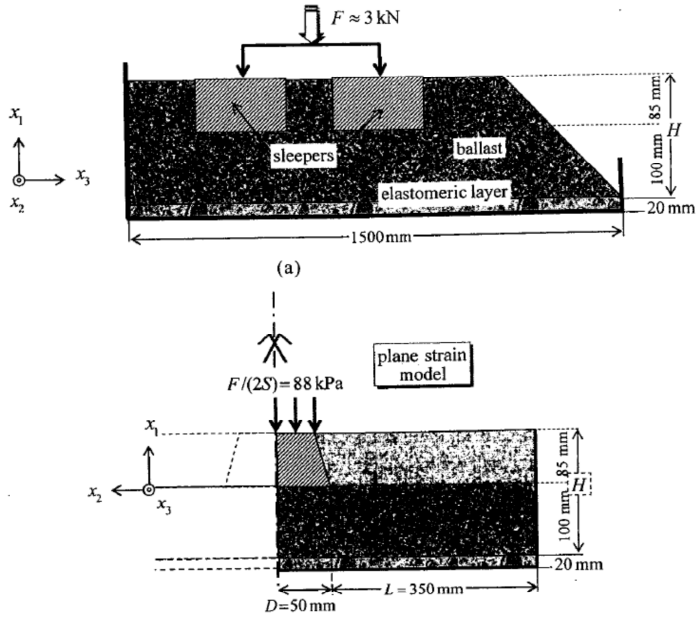

Fig. 10. (a) Schematic transverse cross section of the reduced-scale model of railway track platform (Bodin, 2001) and (b) Longitudinal plane strain calculation model

longer along the Ox_3-axis than along the Ox_2-axis. This plane strain problem is pictured in Fig. 10(b), which gives a cross-sectional view of the reduced scale railway platform in the Ox_1x_2-plane. Exploiting the symmetry of this problem with respect to the plane Ox_1x_3 containing the sleeper, only one half of the structure is shown in this figure, with the appropriate boundary conditions. Since the maximum load applied to the initial structure is $F = 3$ kN, such a loading is simulated in the plane strain problem by applying a uniform pressure of 88 kPa, obtained by dividing the total load F by twice the area S of the sleeper's upper section. A permanent additional pressure of 10 kPa is applied in order to account for the weight of the rail.

A Simplified Analytical Model

An extremely simplified description of the above described test, named "*two-block*" model, has been adopted with the main objective to provide an analytical solution in order to validate the numerical simulation to be carried out. According to this model, only the ballast layer of thickness H located under the sleeper is considered. A uniform pressure varying between 0 and P^m (corresponding to the sleeper's action) is applied on top of it over a width D. This layer is decomposed into two rectangular blocks of respective widths D and $L = \lambda D$ as shown in Fig. 11. The contact between those two blocks is *smooth*, so that, taking into account the boundary conditions, the stress and deformation states are

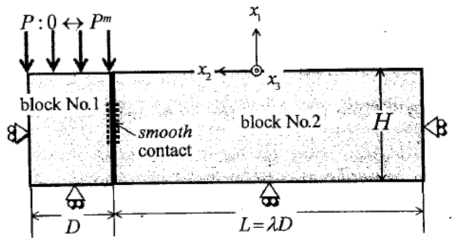

Fig. 11. The "two-block" model

homogenous in each block separately. Moreover, for the sake of simplicity, we assume that permanent deformations are occurring in block No.1 only. The calculation procedure described in Fig. 4 is then applied to this two-block model.

Application of a Preliminary Loading-Unloading Cycle

Starting at $N = 0$ from an initial *stress-free* state, a first loading cycle is applied: the pressure P is increased from 0 to the maximum value P^m, then brought back to zero (*see* Fig. 4). The different notations used in the following analytical developments are defined in Fig. 12.

During the *elastic phase*, the solution reads:

$$\frac{\delta_v}{H} = \frac{P}{E}\left[(1-\nu^2) - \frac{\nu^2(1+\nu)}{1-\nu}\frac{1}{1+\lambda}\right]$$

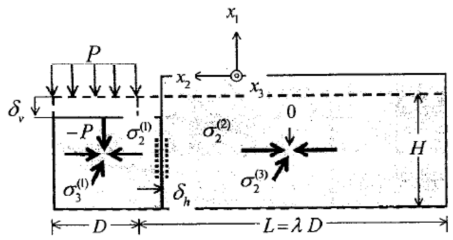

Fig. 12. Stresses and deformations in the "two-block" model

$$\frac{\delta_h}{D}=P\frac{\nu(1+\nu)}{E}\frac{\lambda}{1+\lambda} \tag{32}$$

$$\sigma_2^{(1)}=-\frac{P}{1+\lambda}\frac{\nu}{1-\nu},\ \sigma_1^{(1)}=-P,\ \sigma_3^{(1)}=\nu(-\mathrm{P}+\sigma_2^{(1)}) \tag{33}$$

where δ_v is vertical settlement of block No. 1 and δ_h the horizontal displacement at the interface between the two adjacent blocks.

Assuming that the ballast material is governed by a *Mohr-Coulomb* perfectly plastic criterion, with a cohesion C and friction angle φ, the elastic limit P^e is calculated as follows. Since λ is positive and the Poisson's ration ν is comprised between 0 and 0.5, the principal stresses in block No. 1 are such that:

$$\sigma_1^{(1)}=-P\le\sigma_3^{(1)}\le\sigma_3^{(1)}=-\frac{P}{(1+\lambda)}\frac{\nu}{(1-\nu)} \tag{34}$$

and the yield condition may be written as:

$$(\sigma_2-\sigma_1)+(\sigma_2+\sigma_1)\sin\varphi-2C\cos\varphi\le 0 \tag{35}$$

and consequently

$$P\le\frac{2C\cos\varphi(1-\nu)(1+\lambda)}{(\lambda+1-\nu\lambda)(1-\sin\varphi)-2\nu}=P^e \tag{36}$$

provided that the following condition be fulfilled:

$$(\lambda+1-\nu\lambda)(1-\sin\varphi)-2\nu>0 \tag{37}$$

The *elastoplastic* phase is obtained when P is increased beyond the elastic limit P^e up to the maximum value P^m. It is followed by an elastic unloading phase when P is decreased to zero. The corresponding residual stresses in block No. 1 produced by this first loading/unloading cycle ($N=1$) are:

$$\sigma_1^r(N=1)=0,$$

$$\sigma_2^r(N=1)=(P^e-P^m)\left(\frac{1-\sin\varphi}{1+\sin\varphi}-\frac{\nu}{(1+\lambda)(1-\nu)}\right)$$

$$\sigma_3^r(N=1)=(P^e-P^m)\left[\frac{2\nu}{1-\sin\varphi}-\nu\left(1+\frac{\nu}{(1+\lambda)(1-\nu)}\right)\right] \tag{38}$$

This residual state is considered as the *updated initial state* for the step-by-step calculation procedure (Fig. 4).

Residual State Calculation (Fig. 12)

Let $\Delta\underline{\underline{\varepsilon}}^*(N)$ be the permanent strain increment in block No. 1 generated by the application of ΔN loading cycles between N and $N+\Delta N$:

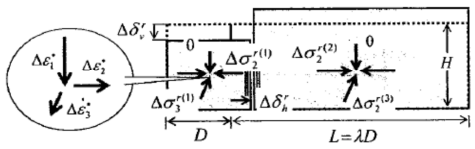

Fig. 13. Residual stress increments due to permanent strain increments in the "two-block" system

$$\Delta\underline{\underline{\varepsilon}}^*(N)=\sum_i\Delta\varepsilon_i^*(N)\underline{\underline{e}}_i\otimes\underline{\underline{e}}_i \tag{39}$$

the corresponding residual stress increments are:

$$k=1,\ 2\quad \Delta\underline{\underline{\sigma}}^{r(k)}=\underline{\underline{\sigma}}^{r(k)}(N+\Delta N)-\underline{\underline{\sigma}}^{r(k)}(N) \tag{40}$$

and the residual strains:

$$\Delta\underline{\underline{\varepsilon}}^{r(1)}=\Delta\underline{\underline{\varepsilon}}^*+\frac{1+\nu}{E}\Delta\underline{\underline{\sigma}}^{r(1)}-\frac{\nu}{E}\mathrm{tr}(\Delta\underline{\underline{\sigma}}^{r(1)})\underline{\underline{1}}$$

$$\Delta\underline{\underline{\varepsilon}}^{r(2)}=\frac{1+\nu}{E}\Delta\underline{\underline{\sigma}}^{r(2)}-\frac{\nu}{E}\mathrm{tr}(\Delta\underline{\underline{\sigma}}^{r(2)})\underline{\underline{1}} \tag{41}$$

Combining all those equations together with the different displacement and stress boundary conditions, finally yields:

$$\frac{\Delta\delta_h^r}{D}=\frac{\lambda}{1+\lambda}(\Delta\varepsilon_2^*+\nu\Delta\varepsilon_3^*),$$

$$\frac{\Delta\delta_v^r}{H}=-\Delta\varepsilon_1^*-\frac{\nu}{(1-\nu)(1+\lambda)}[\Delta\varepsilon_2^*+(1+\lambda-\lambda\nu)\Delta\varepsilon_3^*] \tag{42}$$

where $\Delta\delta_v^r$ and $\Delta\delta_h^r$ are the residual settlement and horizontal displacement increments, respectively, and:

$$\Delta\sigma_2^r=\frac{E}{(1+\lambda)(1-\nu^2)}[\Delta\varepsilon_2^*+\nu\Delta\varepsilon_3^*],\ \Delta\sigma_3^{r(2)}=\nu\Delta\sigma_2^r$$

$$\Delta\sigma_3^{r(1)}=\frac{E}{(1+\lambda)(1-\nu^2)}[\nu\Delta\varepsilon_2^*+(1+\lambda-\lambda\nu^2)\Delta\varepsilon_3^*] \tag{43}$$

the increments $(\Delta p^r, \Delta q^r)$ of the residual stress invariants being calculated from Eq. (43).

Semi-Analytical Simulation

The step-by-step calculation procedure described in Fig. 4, may be implemented in a semi-analytical way, making use of the cyclic constitutive law developed in section 4. The simulation of the structure behaviour is carried out, adopting the following selection of parameters.

◇ Geometry and loading:

$$D=0.05\ \mathrm{m},\ L=\lambda D=0.35\ \mathrm{m},\ P^m=61\ \mathrm{kPa} \tag{44}$$

with $P^m=F/2S'$, where S' is the area of the sleeper's *lower* section.

◇ Material elastic parameters

$$E=250\ \mathrm{MPa},\ \nu=0.3 \tag{45}$$

◇ Cyclic constitutive parameters (Poulmarch's gravel):

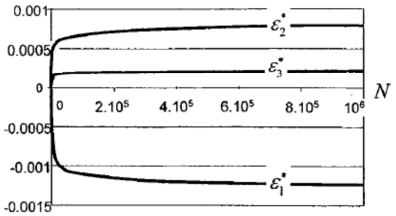

Fig. 14. Evolutions of permanent strain components as functions of N (two-block model)

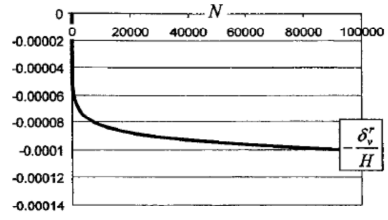

Fig. 15. Evolution of the non-dimensional residual settlement of the "two-block" system

$$\varepsilon_0^* = -0.0195,\ B = 0.03,\ n = 0.588,$$
$$s = 42.8 \text{ kPa},\ m = 3.8 \text{ and } \nu^* = 0.4 \qquad (46)$$

As a result of such a simulation, Fig. 14 represents the evolution of the different permanent strain components in block No. 1 located beneath the applied loading pressure, as functions of the number N of cycles. We can observe that the axial permanent strain is negative (contraction), while the lateral permanent strain is positive (extension), and the third transversal component being slightly positive. The integration of those (non-elastic) strains leads to the calculation of the non-dimensional residual settlement which may be expressed in analytical form as:

$$\frac{\delta_v^r}{H} = -\varepsilon_1^*(N) - \frac{\nu}{(1-\nu)(1+\lambda)} \times [\varepsilon_2^*(N) + (1+\lambda(1-\nu))\varepsilon_3^*(N)] \qquad (47)$$

The curve drawn in Fig. 15 represents the evolution of this residual settlement as a function of N. The settlement increases rapidly in a first stage, then more slowly without any stabilization.

A Necessary Elastoplastic Correction of the Procedure

Analytical as well as numerical simulations performed when following the procedure displayed in Fig. 4, induce a progressive drift of the stress cycle, due to the variation of the residual stress state, which may lead, under certain circumstances, to violate the material yield criterion, or even worse, step over the "reference line", which is clearly physically unrealistic, since it could lead to infinite values of the permanent strains when the maximum loading point is approaching this line. Such a difficulty

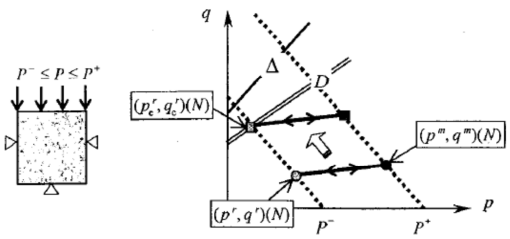

Fig. 16. Cyclic stress paths for the oedometric test

can be overcome by means of an *elastoplastic correction* of the residual state calculation, in which the initially elastic constitutive law should be changed into:

$$\underline{\sigma}^r = \underline{\underline{C}}:(\underline{\varepsilon}^r - \underline{\varepsilon}^* - \underline{\varepsilon}^p),\ \underline{\underline{C}}\text{: elastic stiffness tensor} \qquad (48)$$

where $\underline{\varepsilon}^p$ is the material *plastic* strain, which is classically calculated by means of its yield (Mohr-Coulomb) criterion, along with the plastic flow rule:

$$f(\underline{\sigma}) \le 0 \quad \underline{\dot{\varepsilon}}^p = \dot{\lambda}\frac{\partial g}{\partial \underline{\sigma}}, \quad \dot{\lambda} \ge 0 \qquad (49)$$

where g denotes the plastic potential ($g = f$ in the case of an associated flow rule).

Such a correction of the initial procedure can be illustrated on the example of the *cyclic oedometric test*, in which a homogeneous sample of material placed in a rigid container, is vertically loaded by a uniform pressure varying cyclically between P^- and P^+. Without going into detailed calculations, which may be found in Abdelkrim (2004), the most important results will de commented.

The residual stress being of the form;

$$\underline{\sigma}^r(N) = -P^-\underline{e}_1 \otimes \underline{e}_1 - k(N)P^-(\underline{e}_2 \otimes \underline{e}_2 + \underline{e}_3 \otimes \underline{e}_3) \qquad (50)$$

the elastic cycle is represented in the (p, q)-plane by a segment connecting the residual point of co-ordinates:

$$p^r = -\frac{2}{3}\frac{\nu^*\varepsilon^*}{1-\nu}E + \frac{1+2k_1}{3}P^-,$$
$$q^r = \frac{\nu^*\varepsilon^*}{1-\nu}E + (1-k_1)P^- \qquad (51)$$

with the maximum loading point

$$p^m = p^r + \frac{1+\nu}{3(1-\nu)}(P^+ - P^-),$$
$$q^m = q^r + \frac{1-2\nu}{(1-\nu)}(P^+ - P^-) \qquad (52)$$

where $k_1 = k = (N=1)$, while $\varepsilon^*(N)$ (respectively $-\nu^*\varepsilon^*(N)$) is the vertical (respectively lateral) permanent strain.

Assuming that $\varepsilon^* < 0$ and $\nu^* < 0$, the stress cycle represented by this segment is progressively moving towards the straight line D associated with the material Mohr-Coulomb yield condition, as sketched in Fig. 16. It follows for instance that in the case when the slope of D is

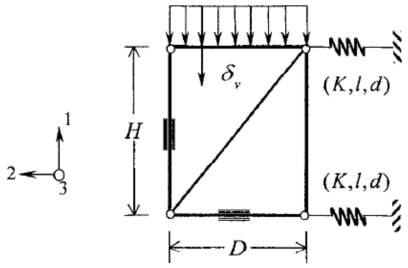

Fig. 17. Finite element modelling of the "two-block" structure

steeper than that of the stress cycle, the residual stress point will first intersect D. The coordinates of the intersecting point are

$$p_e^r=\frac{(3-\sin\varphi)P^- -4C\cos\varphi}{3(1+\sin\varphi)},\quad q_e^r=\frac{3}{2}(P^- -p_e^r) \tag{53}$$

Further calculation of the residual state, incorporating material plastic behaviour, assumes that the stress cycle comes to a stop. A 'thermo" elastic plastic calculation is then carried out, in which the thermal strains are replaced by the permanent strains. It can be shown that, in such a plastic phase, the increment of relative residual settlement as a function of the increment of permanent strain simply writes:

$$\frac{\Delta\delta^r}{H}=-\Delta\varepsilon^*\left[1-2\nu^*\frac{1-\sin\varphi}{1+\sin\varphi}\right] \tag{54}$$

Finite Element Simulation of the "Two-Block" Model

A general numerical tool, incorporating the use of the CESAR-LCPC software as a subroutine for performing the different finite element calculations, has been developed for implementing the algorithm described in Fig. 4, where both the traffic loading and residual calculations have been extended to plasticity (Abdelkrim, 2004). In order to get a first validation of the whole procedure, the previously described "two-block" system has been modelled as indicated in Fig. 17.

Block No. 1 of height H and width L^* is discretized into two three-node triangular elements (T3), while the action of block No.2 is simulated through an equivalent system made of two horizontal arrays of springs applied to the upper and lower right nodes of the mesh. More precisely, denoting by K the spring individual stiffness, l its length and d the space between two springs in the direction normal to the plane of the figure, it can be easily proved that such a spring system behaves in the same way as block No. 2, of height H and length L, provided the following relation be satisfied:

$$k=\frac{K}{dl}=\frac{EH}{2L(1-\nu^2)} \tag{55}$$

For the selected values of the material characteristics and structure geometry, the calculated value of the spring stiffness is $k=35.7$ MN/m^2 for $d=l=1$ m.

NUMERICAL SIMULATION OF THE EXPERIMENTAL TEST: PRELIMINARY RESULTS

Our objective is now to apply the previously elaborated computational tool to the simulation of the test described in Fig. 10(a) and modelled as a plane strain problem (Fig. 10(b)), more specifically trying to reproduce the experimental curves plotting the measured residual settlement of the sleeper as a function of the number of load cycles. Such a calculation is carried out following the general algorithm of Fig. 4, incorporating the material plastic behaviour as indicated in *A Necessary Elastoplastic Correction of the Procedure*. More precisely, assuming that the residual state of the structure due to the application of N load cycles is being known, the determination of this residual state for $N+\Delta N$ cycles is based on the following procedure:

- ◇ elastoplastic residual calculation aimed at integrating the increment of permanent strain field generated by the application of ΔN cycles, no load being applied to the structure;
- ◇ starting from the thus obtained residual state, elastoplastic loading up to the maximum load is carried out, followed by elastic unloading;
- ◇ the extreme states associated with the last elastic unloading sequence constitute the updated residual and maximum loading states.

Since no direct characterization of the constitutive parameters of the ballast material used in the experiments, by means of triaxial tests for instance, was available, the following indirect procedure has been followed. As regards the determination of the ballast elastic properties, a calibration of these parameters has been made in order to get through the finite element simulation the same elastic deflection as the one obtained experimentally by Bodin (2001). The value of E has for instance been taken equal to 50 MPa.

Likewise, the determination of the yield strength characteristics (cohesion C and friction angle φ) has been based on values found in the literature, notably on the experimental results obtained by Indraratna et al. (1998) from large-scale triaxial tests performed on ballast materials. Despite the fact that the intrinsic curve plotted in the Mohr-plane by the authors displays a strong non-linearity, which means that the friction angle is a decreasing function of the mean stress, and that the material does not resist to tensile stresses, the values finally adopted in the simulations were $C=10$ kPa and $\varphi=60°$.

The most important parameters to be introduced in the simulation are those concerning the cyclic behaviour of the ballast. Due to the lack of substantial experimental data relative to the ballast actually used in the experiments, it is proposed, to adapt the constitutive formulation of Gidel et al. (2001) developed for unbound granular materials, the behaviour of which is probably not very different, at least qualitatively, from that of a ballast material. The idea is to calibrate some relevant parameters of this law in order to reproduce by simulation the same results, in terms of residual settlement

evolution, as the ones obtained experimentally.

The difficulty of such an identification procedure lies in the fact that, according to the interpretation of the experimental results made by the authors who performed the experiments (Bodin, 2001; Bodin et al., 2004), the residual settlement is assumed to vary almost linearly beyond a first stage of cycles, that is:

$$\frac{\mathrm{d}\delta_v^r}{\mathrm{d}N} = \text{ct. for } N \geq 25000 \tag{56}$$

where δ_v^r is the vertical residual settlement of the sleeper, whereas the adopted formulation will result in simulated curves displaying the same trend as the local behaviour, that is a variation in $[1-(N/100)^{-B}]$, so that the rate of residual settlement $\mathrm{d}\delta_v^r/\mathrm{d}N$ will progressively decrease. Since we are primarily interested in the evolution of the long term residual settlement, the adjustment is made on the second part of the experimental curves, where it is supposed to vary linearly. Having kept all the other parameters of the cyclic law equal to those identified on the Poulmarch gravel (Gidel et al., 2001), the values of ε_0^* and B for which the simulated curve best fits the experimental one, relative to a particular test (referred to as "Df12d" in Bodin (2001)), are: $\varepsilon_0^* = -0.205$, $B = 0.03$ (*see* Fig. 18). A constant value of $\nu^* = 0.4$ was also selected in the calculations.

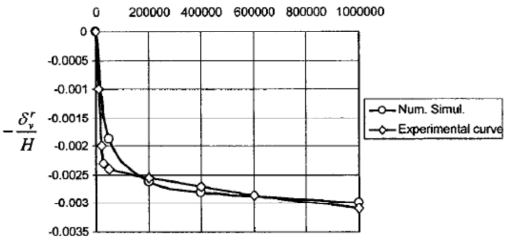

Fig. 18. Calibration of the cyclic law parameters ε_0^* and B on the experimental results

Figure 19 illustrates several aspects of the finite element simulation which has been carried out. The structure is discretized into 226 15-node triangular elements resulting in a mesh of 1893 nodes. Such 15-node triangles prove to be very accurate 2D elements making it possible to produce high quality stress results in spite of the relatively low number of elements. Figures 19(a) and 19(b) represent the residual configurations of the structure after the application of $N = 100$ and 100000 load cycles, respectively (the scale of residual displacements has been magnified for clarity purposes). These pictures clearly show that, as could be expected, the maximum residual settlement (which is denoted by δ_v^r) is obtained in the central part of the structure where the loading is applied, whereas a significant upheaval seems to appear in the vicinity of the lateral boundaries. The residual stress field corresponding to the configuration of Fig. 19(b) is shown in Fig. 19(c), where the principal stresses are reported along with the principal directions of the stress tensor. This stress field corresponds to the sum of the stresses induced by the non-elastic deformations and of the permanent stresses due to the weight of the rail. The maximum stress values are obtained in the vicinity of the

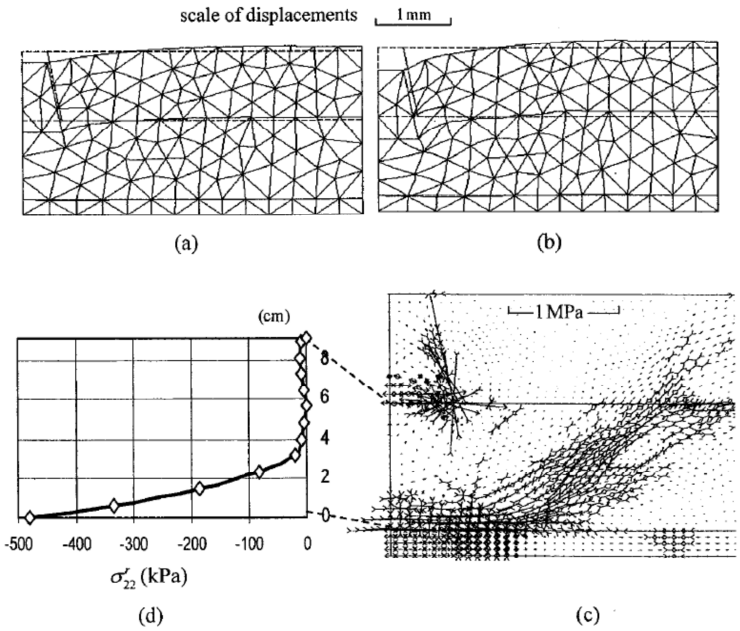

Fig. 19. Residual configuration of the railway track model due to the application of (a) 100 cyles and (b) 100000 cycles: (c) Residual stress distribution associated with the latter configuration and (d) horizontal residual stress profile in the ballast layer underneath the sleeper

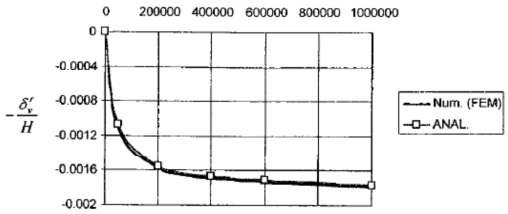

Fig. 20. Numerical vs. semi-analytical simulations of the "two-block" system

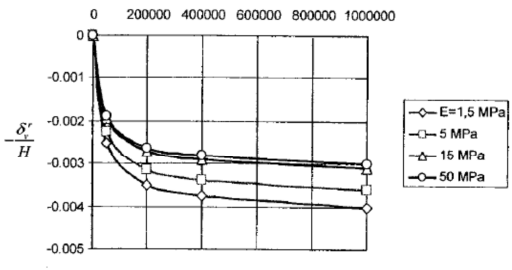

Fig. 21. Influence of the underlying elastomer stiffness on the evolution of the residual settlement (FEM simulations)

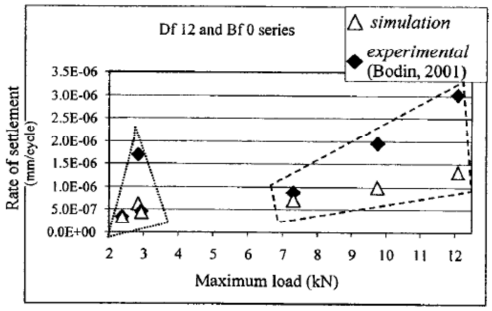

Fig. 22. Rate of residual settlement per cycle as a function of applied load: comparison between simulated and experimental results

sleeper's right hand corner, as well as in the lower central part of the ballast layer, just above the elastomeric layer. As it is clearly apparent from Fig. 19(d), which displays the profile of the horizontal stress component along the vertical segment connecting the sleeper to the elastomeric layer, such residual stresses are predominantly compressive, up to several hundreds of kPa.

As can be seen in Fig. 20, which displays the finite element simulation of the "two-block" model, together with that obtained through the semi-analytical procedure described in section 5, both simulations being carried out with the previously calibrated parameters, the corresponding curves are almost coincident, thereby providing a validation of the numerical tool. Furthermore, comparison of curves displayed in Figs. 18 and 20 show that, in spite of its extreme simplicity, the two-block model produces a rough estimate for the non-dimensional residual settlement, namely 0.0018, instead of 0.003 for 1 million applied load cycles.

The influence of the subgrade soil stiffness, represented by the elastomeric layer, on the evolution of the residual settlement is represented in Fig. 21. It clearly appears that increasing the elastomer Young's modulus results in a reduction of the residual settlement, although such an influence is not so important, since the relative residual settlement obtained for 1 million applied load cycles is about 0.003 for a 50 MPa elastomer, instead of 0.004 for a much softer elastomer (1.5 MPa).

Retaining the previously identified set of constitutive parameters, a further comparison has been made between the results of the numerical simulation and other experimental tests performed by Bodin (2001). The comparison was more specifically focused on the slope of the different curves in their second stage of evolution, which represents the *rate of residual settlement per cycle* $\mathrm{d}\delta_v^r/\mathrm{d}N$, expressed in mm per cycle.

The results of this comparison are reported in Fig. 22, in the form of points representing the values of the calculated or measured rates of settlement as functions of the maximum applied vertical load. Two groups of points corresponding to two different series of tests have been plotted. In the first group of three tests, which includes the calibration test (superposed simulated and experimental points located in the lower left corner of the figure), the maximum applied load was about 2–3 kN, while the second group of points corresponds to the application of a significantly higher load level (7–12 kN).

Such a comparison suggests the following comments.

- ◇ In the first series of tests, one may observe a considerable scattering of experimental points, which is not the case of numerical simulations, even though a certain numerical instability appears, which may probably be attributed to a problem of convergence of elastoplastic calculations, due to the very high friction angle adopted for the ballast material.
- ◇ The second group of points, located on the right-hand side of the graphics, confirms the experimental trends according to which the rate of residual settlement is an increasing function of the applied load, although the numerical predictions seem to significantly underestimate the experimental results.

CONCLUDING REMARKS

This contribution has presented a general procedure, based on structural analysis, for predicting the long term settlement of a railway platform or road pavement subject to traffic loading. The feasibility of such a method has been shown both on illustrative analytical examples and on more realistic configurations, such as in the simulation of a reduced scale experimental bench test, even though in the latter case it does not represent a complete validation of the method, since it was necessary to calibrate some of the relevant parameters of the cyclic constitutive law used in the numerical simulation. In order to improve its predictability, this procedure and

related computational tool, remain to be upgraded on several points.

It should first be extended to the treatment of really three dimensional problems, which was the case of the experiments conducted on reduced or full scale models, such as the experiments which have been simulated in the paper by resorting to a simplified plane strain description. This would require the use of adequate finite element or boundary element computer codes.

The whole procedure has been carried out within the framework of quasi-static evolutions, that is neglecting all dynamic effects. While this certainly proves a valid assumption when the cyclic loading is applied at a relatively low frequency, such dynamic effects should be taken into account for higher frequencies, which may be associated for instance in the situation of very high speed trains. Having neglected such dynamic effects might be one important factor which could explain the observed discrepancy between numerical (quasi-static) simulations and experimental results in which the loading frequency was relatively high (1 to 10 Hz). Those dynamic effects are likely to induce significant modifications of the stress cycles generated by the moving load, both in terms of amplitude and position in the stress space, which could be incorporated in the general procedure described in Fig. 4 by performing elasto*dynamic*, instead of elasto*static* calculations for determining, the traffic load-induced solicitations in the platform, while the other components of this procedure (cyclic constitutive law, residual calculation) would remain unchanged.

More importantly, since one of the key ingredients of the computational procedure, is the formulation of a cyclic constitutive law relating the production of permanent strains in the materials to the characteristics of the stress cycles, a quite significant effort should be devoted in the future to the achievement of such a reliable formulation on the basis of an extensive experimental program, as it has been done for instance by Wichtmann et al. (2004) in the case of sands. One of the important elements of such a cyclic constitutive formulation would be its ability to account for cyclic loadings where the principal directions of the stress rotate, which is obviously a characteristic feature of moving loads (*see* the simplified model treated in Abdelkrim et al., 2003). As regards more specifically the cyclic behaviour of ballast materials, such experiments should involve the use of large triaxial test facilities, in order to avoid possible scale effects due to the typical grain size of this kind of granular materials.

REFERENCES

1) Abdelkrim, M. (2004): A structural analysis approach to predict the long term behaviour of traffic platforms, *PhD Thesis*, ENPC, France (in French).
2) Abdelkrim, M., Bonnet, G. and de Buhan, P. (2002): A numerical method for predicting the residual settlement of railroad track under repeated traffic loading, *Num. Meth. Geotech. Engrg.* (ed. by Mestat), Presses de l'ENPC-LCPC, Paris, 125–130.
3) Abdelkrim, M., Bonnet, G. and de Buhan, P. (2003): A numerical method for predicting the long term residual settlement of a platform induced by repeated traffic loading, *Comput. Geotech.*, **30**, 463–476.
4) Alva-Hurtado, J. H. D. (1980): A methodology to predict the elastic and inelastic behaviour of railroad ballast, *PhD Thesis*, University of Massachusetts.
5) Bodin, V. (2001): Analysis of the global response of a ballast railway track under vertical and lateral loading, *PhD Thesis*, ENPC, Paris (in French).
6) Bodin, V., Sab, K., Tamagny, P. and Gautier, P. E. (2004): Experimental determination of a ballast lateral settlement law, *Cyclic Behav. Soils and Liquefaction Phenomena* (ed. by Triantafillydis), A. A. Balkema, 619–625.
7) Boyce, H. R. (1980): A non linear model for the elastic behaviour of granular materials under repeated loading, *Int. Symp. Soils under Cyclic and Transient Loading*, Swansea, **1**, 285–294.
8) Chai, J. C. and Miura, N. (2002): Traffic-load-induced permanent deformation of road on soft subsoil, *J. Geotech. Engrg.*, **128**(11), 907–916.
9) Dormieux L., Auriault J. L. and Coussy, O. (1993): Pore pressures generation in a seabed subjected to wave loading, *Eur. J. Mech.*, A /Solids, **12**(6), 773–801.
10) Gidel, G., Hornych, P., Chauvin, J. J., Breysse, D. and Denis, D. (2001): Nouvelles approches pour l'étude des déformations permanentes des graves non traitées à l'appareil triaxial à chargements répétés, *Bull. liaison P.Ch.*, **233**, 5–21.
11) Guérin, N. (1996): Experimental and numerical approach to the behaviour of railway ballast, *PhD Thesis*, ENPC, Paris (in French).
12) Hornych, P., Corte, J. F. and Paute, J. L. (1993): Etude des déformations permanentes sous chargements répétés de trois graves non traitées, *Bull. liaison P. Ch.*, **184**, 45–55.
13) Hornych, P., Kazaï, A. and Piau, J. M. (1998): Study of the resilient behaviour of unbound granular materials, *Proc. BCRA 98 Conf.*, Trondheim, 3, 1277–1287.
14) Indraratna, B. and Salim, W. (2003): Deformation and degradation mechanics of recycled ballast stabilised with geosynthetics, *Soils and Foundations*, **43**(4), 35–46.
15) Indraratna, B., Ionescu, D. and Christie, H. D. (1998): Shear behaviour of railway ballast based on large scale triaxial tests, *J. Geotech. Geoenv. Engrg.*, **124**(5), 439–449.
16) Lekarp, F. and Dawson, A. (1998): Modelling permanent deformation behaviour of unbound granular materials, *Construction and Building Materials*, **12**(1), 9–18.
17) Li, D. and Selig, E. T. (1996): Cumulative plastic deformation for fine-grained subgrade soils, *J. Geotech. Engrg.*, **122**(12), 1006–1013.
18) Li, D. and Selig, E. T. (1998): Method for railway track foundation design, II: application, *J. Geotech. Engrg.*, **124**(4), 323–329.
19) Monosmith, C. L., Ogawa, N. and Freeme, C. R. (1975): Permanent deformation characteristics of subsoil due to repeated loading, *Trans. Res. Rec.*, **537**, 1–17.
20) Niemunis, A., Wichtmann, T. and Triantafyllidis, Th. (2004): Explicit accumulation model for cyclic loading, *Cyclic Behav. Soils and Liquefaction Phenomena* (ed. by Triantafillydis), A. A. Balkema, 65–76.
21) Niemunis, A., Triantafyllidis, Th. and Wichtmann, T. (2005): A high-cycle accumulation model for sand, *Comp. Geotech.*, **32**, 245–263.
22) Pecker, A., Prevost, J. H. and Dormieux, L. (2001): Analysis of pore pressure generation and dissipation in cohesionless materials during seismic loading, *J. Earthq. Engrg.*, **5**(4), 441–464.
23) Raymond, G. P. and Williams, D. R. (1978): Repeated load triaxial tests on a dolomite ballast, *J. Geotech. Engrg.*, **104**, 1013–1029.
24) Wichtmann, T., Niemunis, A. and Triantafyllidis, Th. (2004): Strain accumulation in sand due to drained uniaxial cyclic loading, *Cyclic Behav. Soils and Liquefaction Phenomena* (ed. by Triantafillydis), A. A. Balkema, 233–246.
25) Wichtmann, T., Niemunis, A. and Triantafyllidis, Th. (2005): Strain accumulation in sand due to cyclic loading: drained triaxial tests, *Soil Dynam. Earthq. Engrg.*, **25**, 967–979.